A plausible model of phyllotaxis

Richard S. Smith*†, Soazig Guyomarc'h†‡, Therese Mandel‡, Didier Reinhardt‡§, Cris Kuhlemeier‡, and Przemyslaw Prusinkiewicz*¶

*Department of Computer Science, University of Calgary, 2500 University Drive NW, Calgary, AB, Canada T2N 1N4; and ‡Institute of Plant Sciences, University of Berne, CH-3013 Berne, Switzerland

A striking phenomenon unique to the kingdom of plants is the regular arrangement of lateral organs around a central axis, known as phyllotaxis. Recent molecular-genetic experiments indicate that active transport of the plant hormone auxin is the key process regulating phyllotaxis. A conceptual model based on these experiments, introduced by Reinhardt *et al.* [Reinhardt, D., Pesce, E. R., Stieger, P., Mandel, T., Baltensperger, K., *et al.* (2003) *Nature* **426,** 255–260], provides an intuitively plausible interpretation of the data, but raises questions of whether the proposed mechanism is, in fact, capable of producing the observed temporal and spatial patterns, is robust, can start *de novo*, and can account for phyllotactic transitions, such as the frequently observed transition from decussate to spiral phyllotaxis. To answer these questions, we created a computer simulation model based on data described previously or in this paper and reasonable hypotheses. The model reproduces, within the standard error, the divergence angles measured in *Arabidopsis* seedlings and the effects of selected experimental manipulations. It also reproduces distichous, decussate, and tricussate patterns. The model thus offers a plausible link between molecular mechanisms of morphogenesis and the geometry of phyllotaxis.

active transport | auxin | PIN | polarity | computer simulation

Within the variety of phyllotactic patterns found in nature, the most intriguing and, at the same time, the most prevalent is the spiral phyllotactic pattern characterized by the arrangement of organs into conspicuous spirals (parastichies), where the numbers of parastichies are consecutive elements of the Fibonacci series. This pattern is related to the divergence angle between organs approximating the golden angle of 137.5°. In the entire world of developmental biology, phyllotaxis is perhaps the most striking example of a phenomenon that can only be described by using quantitative notions of geometry.

The regularity and mathematical properties of spiral phyllotaxis have attracted the attention of biologists and mathematicians since the early 19th century. They proposed conceptual, mathematical, and computational models, which elucidated the geometric properties of spiral phyllotactic arrangements (1) and the emergence of phyllotactic patterns during plant development. This latter category of models was pioneered by Hofmeister (2) and Snow and Snow (3), who hypothesized that the creation of new primordia is inhibited by the proximity of older primordia. New primordia, therefore, can be formed only at a certain minimal distance from the old ones. This general hypothesis has subsequently been refined into a number of computational models, postulating and exploring different types of inhibitory mechanisms such as geometric spacing (4), physical forces (5, 6), and chemical signals (7, 8).

In the absence of molecular data, the proposed mechanisms were more or less abstract. Recent experiments, however, provided an insight into the molecular processes involved in phyllotaxis, pointing to the central role of active transport of the plant hormone auxin. When shoot apices were cultivated in the presence of auxin transport inhibitors, the induction of lateral organs was blocked, and the apices grew vigorously as radially symmetric structures. Application of the natural auxin indole-3-acetic acid (IAA) to such pin-shaped meristems induced lateral primordia, with the size and

position depending on the concentration and the position of the applied auxin (9). Furthermore, the cellular distribution and subcellular localization of the auxin efflux facilitator PIN1 was consistent with a role in organ positioning (10).

On the basis of these data, Reinhardt *et al.* (10) proposed a conceptual model of phyllotaxis (ref. 10; Fig. 1). According to this model, auxin is transported acropetally toward the meristem, where it is redirected to the primordia, which function as sinks. As a result, auxin is depleted from the surroundings of the primordia and reaches the organogenetic peripheral zone only at a certain minimal distance from the two youngest primordia (P1 and P2). Auxin accumulates at this position, where it induces a new primordium (incipient primordium I1) that, in the course of the plastochron, grows out and becomes a sink itself. The phyllotactic pattern thus results from the dynamics of interaction between existing and incipient primordia in a growing apex, mediated by the actively transported auxin.

The mechanism proposed by Reinhardt *et al.* (10) is plausible in the sense that it is consistent with the available molecular data and captures qualitatively the inhibitory effect of the existing primordia on an incipient primordium. However, the question of whether it is indeed capable of generating the highly constrained geometry of spiral phyllotactic patterns was open. We answer this question by constructing a simulation model. It is based on data concerning the induction of primordia by high auxin concentrations and the polar localization of the auxin transport facilitator PIN1 in the surface layer of the apex (10). We also include previously undescribed experimental data focused on the distribution of auxin in the meristem and the incipient primordia. The ensuing model shows that the molecular mechanisms identified by Reinhardt *et al.* (10) and further developed in this paper can lead to the formation of the phyllotactic patterns observed in nature.

Experimental Results

Previously published data in refs. 9–12 formed the initial experimental basis for the model. To meet the needs of model construction, we also acquired additional data, focused on the localization of auxin within the meristem and the incipient primordia.

Data Set 1: Phyllotactic Patterning Occurs in the Outer Layer of the Shoot Meristem (L)1. The PIN1 protein is located primarily, although not exclusively, in the external L1 layer (figure 1*A* and *C* in ref. 10). This localization suggests that phyllotactic patterns may be formed essentially on the surface of the shoot apical meristem. To examine this hypothesis, we considered transgenic plants containing the *DR5::GFP* reporter construct, which is thought to reflect endogenous auxin concentrations (12, 13). The expression of *DR5::GFP* in the meristem was confined to the L1 layer (Fig. 2*A*). The auxin may
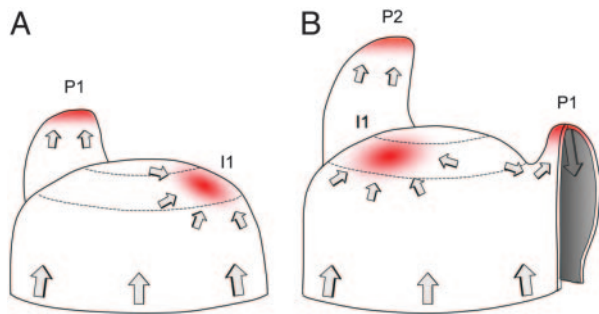
DEVELOPMENTAL BIOLOGY

Fig. 1. Conceptual model of the regulation of phyllotaxis by polar auxin fluxes in the shoot meristem. Adapted from ref. 10. (*A*) PIN1 orientation directs auxin fluxes (arrows) in the L1 layer, leading to accumulation of auxin (red color) at the initiation site (I1) in the peripheral zone. This accumulation eventually results in organ induction. (*B*) Later, basipetal PIN1 polarization inside the bulging primordium (P1) drains auxin into inner layers, depleting the neighboring L1 cells. As a consequence, another auxin maximum is created in the peripheral zone at position I1 removed from primordia P1 and P2.

be retained in the L1 by auxin transporters, most importantly AUX1, which is strictly localized to the L1 (10, 14).

Control experiments showed that even after exogenous application of the synthetic auxin sirtinol, thought to bypass auxin transport (15), cells in the inner layers L2 and L3 did not stain well for GFP (Fig. 2*B*). One possibility is that an active product of sirtinol, for example 1-naphthoic acid (15), could be subject to active transport impeding its spread to L2 and L3 in a manner similar to auxin. Summarizing these results, we limited our simulations to the L1, considering internal layers only at the sites of primordia (see Data Set 5).

Data Set 2: Auxin Is Readily Available Throughout the Meristem. Further questions concern the sites of auxin synthesis, inactivation, and turnover. These processes are surprisingly complex, because multiple pathways contribute to auxin homeostasis (16, 17). According to our 2003 model (10), auxin is not produced in the meristem but imported from basal tissues. If this hypothesis were true, inhibition of auxin transport should lead to a depletion of auxin in the meristem. To test this hypothesis, we inhibited auxin transport by using either the *pin1* mutant background or the transport inhibitor *N*-1-naphthylphthalamic acid (NPA). In the *pin1* mutant, the *DR5::GFP* expression was indeed extremely low (Fig. 2*C*), whereas after the application of NPA, the *DR5::GFP* expression remained high. Nevertheless, after NPA application, the phyllotactic pattern observed in wild-type meristems disappeared, and a ring of *DR5::GFP* expression was observed instead (compare Fig. 2 *D* and *F* with Fig. 6 *L* and *B*, which is published as supporting information on the PNAS web site).

The *pin1* mutant lacks lateral organs, presumptive sites of auxin synthesis (10). In contrast to the short-term effect of NPA, the lack of *DR5::GFP* expression in *pin1* meristems is likely to reflect the cumulative effect of compromised active auxin transport over a prolonged time. Thus, at the time scale of minutes to hours, which is relevant for phyllotactic patterning, auxin may be readily available throughout the meristem, even if the transport mechanism is impeded. This observation is consistent with the recent work on *Arabidopsis* embryos, according to which experimental interference with auxin synthesis and conjugation does not greatly influence auxin distribution (18). In conclusion, we now assume nonlocalized auxin synthesis and turnover throughout the surface of the peripheral zone. PIN1 function is required to maintain the unequal distribution of auxin, which is the essence of phyllotactic pattern formation.
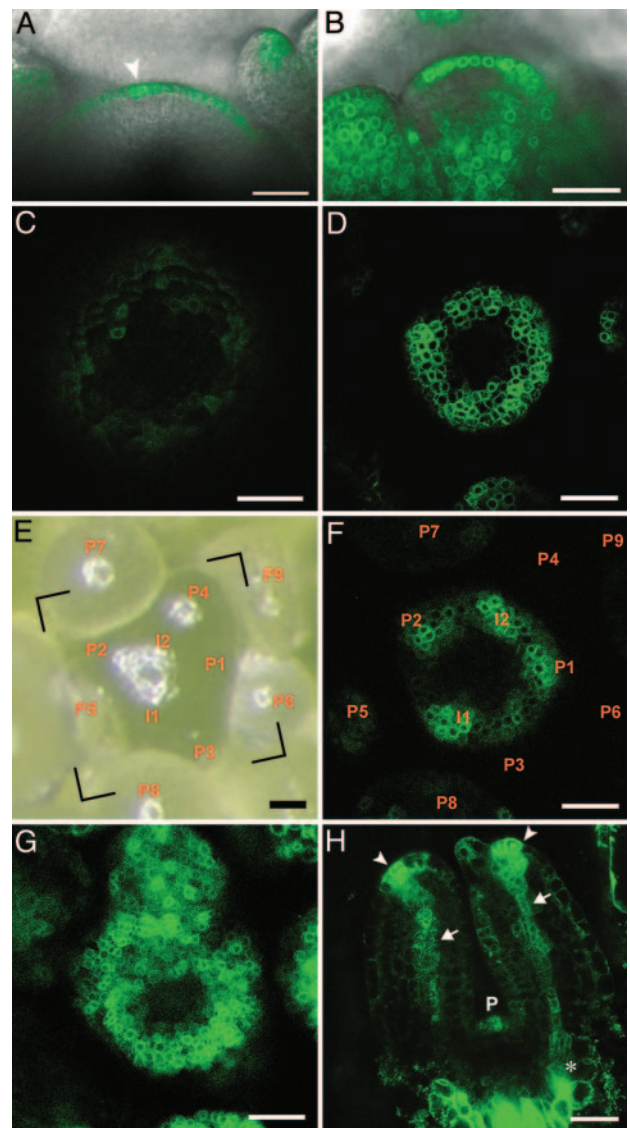

Fig. 2. *DR5::GFP* expression in the shoot apex. (*A*) Longitudinal section of a *DR5::GFP*-expressing wild-type inflorescence meristem. The arrowhead indicates local overexpression of *DR5::GFP* consistent with an initial. (*B*) Longitudinal section of a *DR5::GFP*-expressing wild-type inflorescence meristem treated with 25 μM sirtinol during 48 h. (*C*, *D*, *F*, and *G*) Transverse confocal pictures, taken with comparable settings. (*C*) *DR5::GFP* expression pattern in a *pin1-7* inflorescence meristem. (*D*) *DR5::GFP* expression pattern in a wild-type inflorescence meristem treated with 20 μM NPA during 24 h. (*E*) Top view of a wild-type inflorescence meristem, visualized with a binocular microscope. (*F*) Transverse confocal picture showing the *DR5::GFP* expression pattern in the same meristem as shown in the frame indicated in *E*. Spots of GFP signal are observed in the peripheral zone of the meristem where no bulge is visible (compare to *E*). (*G*) *DR5::GFP* expression pattern in a wild-type inflorescence meristem treated with 25 μM sirtinol during 48 h. (*H*) Longitudinal view of the two first, 3-day-old, leaf primordia of a *DR5::GFP*-expressing seedling. Note the strong signals at the tips of the primordia (arrowheads), and *DR5::GFP* expression in the future midveins (arrows), which connect with the stem vasculature (asterisk). P indicates the *DR5::GFP* expression in the next primordium. (Scale bars: 25 μm.)

Data Set 3: PIN1 Expression is Up-Regulated by Auxin. It has been shown that auxin regulates the expression of PIN proteins in the root (19). This result suggests that auxin may regulate the expression of PIN1 in the shoot meristem as well. Analysis of transversal sections (Figs. 2 *E* and *F* and 6 *A–E*) shows that *DR5::GFP* expression peaks in incipient primordia. After sirtinol treatment,

however, all cells of the L1, including those in the central zone of the meristem, express *DR5::GFP* at equal levels (Fig. 2*G* and 6 *F–J*). These observations indicate that all cells in the L1 are auxin-responsive and that within the L1, the *DR5::GFP* expression levels are likely reflecting endogenous auxin concentrations. Because the maxima of PIN1 expression are also located at the sites of incipient primordia (10, 12), we assume that auxin positively regulates PIN1 expression in the meristem.

Data Set 4: PIN1 Is Polarized by Auxin. Given the role of PIN proteins as facilitators of polar transport, their localization in the cell is of primary importance. In the L1, PIN1 is polarized toward the incipient primordia (figure 1*C* in ref. 10), in which auxin concentration appears to reach a maximum. On this basis, we hypothesize that PIN1 in the L1 is preferentially polarized toward the neighboring cells with the highest auxin concentration. The form and extent of this polarization have been obtained by searching the parameter space of the model. Although this assumption has no direct experimental foundation, the molecular mechanism is likely to involve two elements: (*i*) auxin-modulated endocytosis of PIN1 (20), and (*ii*) a mechanism that informs cells about auxin concentration in their neighbors, for example, by measuring extracellular auxin or via a receptor-ligand system.

Data Set 5: Auxin Is Exported from Primordia to Subepidermal Layers. Strong PIN1 expression in the primordia (10) coincides with the strands of high expression of the *DR5::GFP* reporter construct, which persist during organ outgrowth and become connected to the central vasculature (Fig. 2*H*; refs. 21 and 22). This observation suggests that primordia act as sites of auxin export from the L1 to the central vasculature. The capacity of AUX1 to retain auxin in the L1 may be exceeded at I1, where it "escapes" into internal layers and induces organ identity and organ outgrowth (10, 14). In summary, we assume that primordia can act as sinks of auxin in the L1 despite the high concentration and, possibly, production of auxin in the primordia. These functions can be combined at the same site because of the polar character of auxin transport.

Simulation Model

Key Assumptions. We distilled the experimental results and hypotheses underlying our model into the following assumptions.

(*i*) Phyllotactic pattern formation is a dynamic process, driven by the growth of the shoot apical meristem.

(*ii*) The L1 functions as an isolated conduit for auxin transport in the patterning of the shoot apical meristem (Data Set 1).

(*iii*) Auxin is readily available in the L1 because of flow from the lower parts of the shoot and/or local production (Data Set 2).

(*iv*) Auxin is redistributed in the L1 by a combination of diffusion and active transport mediated by PIN1 molecules (Data Set 2).

(*v*) PIN1 concentration in a cell is up-regulated by auxin (Data Set 3).

(*vi*) PIN1 localization in the cells is determined by the concentration of auxin in the neighboring cells (Data Set 4).

(*vii*) Only the peripheral zone, the band of cells below the apex, is competent to induce lateral organs in response to auxin (9).

(*viii*) A new primordium emerges at the location of high concentration of auxin (see Fig. 2 *E* and *F* and Data Set 3; refs. 10 and 12).

(*ix*) Incipient primordia acquire new developmental identity (23), which may modify model parameters compared to the intervening regions.

(*x*) Despite high auxin levels, primordia act as sinks for auxin in the L1, as the auxin is pumped into the internal layers, initiating vasculature (Data Set 5).

These assumptions form the foundation for three components of the model: a geometric model of a growing meristem (*i* and *ii*) described in *Supporting Text* and Fig. 7, which are published as supporting information on the PNAS web site, a model of cell polarization and auxin transport (*iii–vi*), and an integrated model of phyllotaxis (*vii–x*).

Model of Cell Polarization and Auxin Transport. At the heart of the model lies the interaction between four factors: the overall concentration of PIN1 within the cell, allocation of PIN1 proteins to individual cell membranes, transport of IAA (auxin) between a cell and its neighbors, and changes in IAA concentration. These factors form a feedback loop, in the sense that the concentration and localization of PIN1 proteins in a cell depend on the concentration of IAA in this cell and its neighbors, whereas the IAA concentrations are changing as the result of fluxes dependent on the concentration and localization of PIN1 proteins (Fig. 8, which is published as supporting information on the PNAS web site). To test whether these assumptions can lead to a plausible simulation model, capable of recreating the observed phenomena at the cellular level (dynamics of PIN1 polarization and auxin distribution) and whole-meristem level (emergence of a phyllotactic pattern), we quantified these assumptions by using a set of equations.

The number of PIN1 proteins in a cell *i* is assumed to change according to the formula

$$\frac{d[PIN]_i}{dt} = production - decay$$

$$= \frac{\rho_{PIN_0} + \rho_{PIN}[IAA]_i}{1 + \kappa_{PIN}[PIN]_i} - \mu_{PIN}[PIN]_i, \quad [1]$$

where ρ_{PIN_0} is the base production, ρ_{PIN} is a coefficient capturing the up-regulation of PIN1 production by auxin, κ_{PIN} controls saturation of PIN1 production at high concentrations, and μ_{PIN} is the decay constant.

PIN1 proteins are distributed between cell membranes according to the formula

$$[PIN]_{i \to j} = \frac{[PIN]_i l_{i \to j} b^{[IAA]_j}}{\sum_j l_{i \to j} b^{[IAA]_j}}, \quad [2]$$

where $[PIN]_{i \to j}$ is the number of PIN1 proteins located in the membrane of cell *i* near the wall that separates it from cell *j*, and $l_{i \to j} = l_{j \to i}$ is the length of the wall that separates cells *i* and *j*. The exponentiation base $b > 1$ controls the extent to which PIN1 protein distribution is affected by the neighboring cells. In the absence of experimental data, we tested a number of alternative formulas and found that the postulated exponential dependence of the localization of PIN1 on the concentration of IAA results in the most stable phyllotactic patterns.

The effect of PIN1 proteins on the efflux of auxin from cell *i* to a neighboring cell *j* is modeled by using the formula

$$active\_transport_{i \to j} = T[PIN]_{i \to j} \frac{[IAA]_i^2}{1 + \kappa_T[IAA]_j^2}, \quad [3]$$

where T is a polar transport coefficient, and κ_T is a transport saturation coefficient. For a given number of PIN1 molecules near the wall separating cell *i* from cell *j*, the flux of auxin from *i* to *j* is thus assumed to increase with the concentration of auxin in cell *i* and saturate with an increasing concentration of auxin in cell *j*. The quadratic dependence of the flux on these concentrations is not based on experimental data. However, in the simulations, it was found to provide better control over the spacing of peaks in the resulting patterns than linear relations.
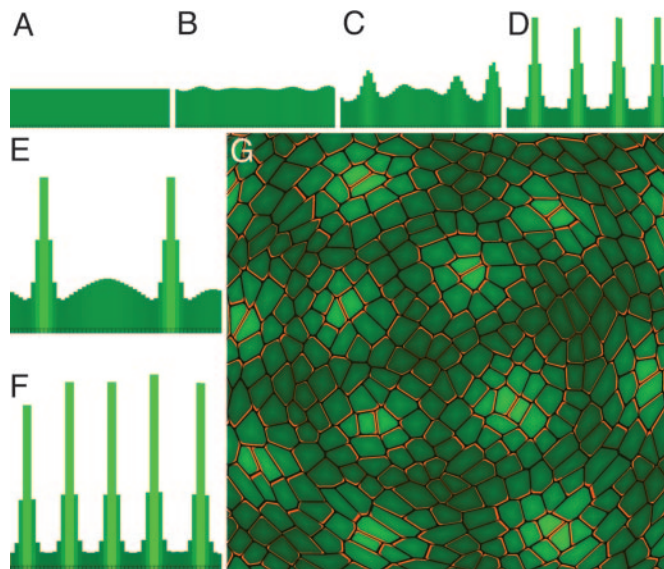
Fig. 3. Pattern generation by the transport-based model. (*A–D*) Pattern emergence in a sequence of 50 cells with wraparound boundary conditions (the leftmost and the rightmost cell are considered neighbors). Taller bars (brighter green) indicate higher IAA concentration. Simulation steps 30, 60, 70, and 80 are shown. A small amount of noise present in the initial distribution is required to break symmetry. (*E* and *F*) Pattern dependence on model parameters. Model parameters affect how many peaks a given number of cells will create. Higher values of the transport coefficient result in more peaks. If the transport coefficient is too low, no peaks will form at all. Transport coefficient: A-D, 4.0; E, 3.0; F, 10.0. (*G*) Pattern formed in a simulated cellular structure. PIN1 is depicted in red.

Finally, the changes in IAA concentration in a cell *i* are modeled by the equation

$$\frac{d[IAA]_i}{dt} = production - decay + diffusion$$
$$+ \sum_j (-active\_transport_{i \to j} + active\_transport_{j \to i}),$$

$$[4]$$

where the first three terms are expressed as

$$production - decay + diffusion$$

$$= \frac{\rho_{IAA}}{1 + \kappa_{IAA}[IAA]_i} - \mu_{IAA}[IAA]_i - \sum_j D_j([IAA]_i - [IAA]_j). \quad [5]$$

In the above equation, the rate of auxin production is assumed to decrease from the maximum value ρ_{IAA} as the auxin concentration increases, with κ_{IAA} controlling saturation. Auxin decay is controlled by the decay constant μ_{IAA}. Diffusion takes place directly between neighboring cells (intercellular space is ignored), with the cell membranes representing the main obstacle to diffusion. Each of the diffusion coefficients D_j is proportional to the membrane length between a given cell and its *j*th neighboring cell.

The above model depends on active transport of a morphogenetic substance and, thus, is fundamentally different from reaction-diffusion models (8, 24). To test the pattern-formation capability of this model, we applied it to a row of cells connected at the ends to form a ring and to a two-dimensional cellular structure (Fig. 3). In both cases, a stable pattern of approximately equally spaced peaks of auxin concentration emerged from an initially homogeneous distribution with small initial perturbations. The amplitude and

spacing between these peaks could be controlled by manipulating model parameters (Fig. 3 *D–F*), with decreased transport leading to fewer peaks and increased transport leading to more peaks. Thus, the interaction between auxin concentration and transport provides a patterning mechanism.

Model of Phyllotactic Patterning. We initially hypothesized that phyllotaxis in *Arabidopsis* is determined directly by the transport-based patterning mechanism, operating on the growing surface of the apical meristem. In simulations, however, we were not able to obtain sustained spiral phyllotactic patterns by using that mechanism alone, although patterns of irregularly spaced primordia could easily be generated. This observation was upheld by numerous simulations, in which we used diverse parameter values and different formulas for polarizing PIN1. We thus concluded that additional factors play an important role in the generation of phyllotactic patterns in Arabidopsis. To test this hypothesis, we extended the transport-based patterning model with the following elements, which are related to key assumptions *vii–x*.

(*i*) The surface of the apex is divided into the central zone, peripheral zone, and proximal zone (located below the peripheral zone). Auxin production depends on the zone in which a cell is located. No auxin is produced in the central zone. The coefficients controlling auxin production are different in the peripheral and proximal zones, with ρ_{IAA}(*peripheral*) being greater than ρ_{IAA}(*proximal*).

(*ii*) The peripheral zone is divided into primordia and intervening regions (between the primordia). A primordium is initiated when the IAA concentration in two adjacent cells reaches a predefined threshold *Th*. The primordium center is located at the midpoint of the centroids of these two cells. Radius *r* increases with time (Fig. 7*A*) according to a predefined function.

Primordia cells are differentiated from the intervening regions of the shoot apical meristem, which has three consequences.

(*i*) The differentiated cells produce auxin at a relatively higher rate

$$additional\ production = \frac{\rho_{IAA}(primordium)}{1 + \kappa_{IAA}[IAA]_i}\left(1 - \frac{d_i}{r}\right), \quad [6]$$

where d_i is the distance of the centroid of a primordium cell *i* from the primordium center.

(*ii*) Polarization of PIN1 proteins toward the primordium center is increased, compared to the intervening region. This increase is achieved by using an "auxin-concentration equivalent," $[IAA']$, instead of the current auxin concentration, as the polarizing factor. The auxin-concentration equivalent is defined as

$$[IAA']_i = \max\left\{[IAA]_i, [IAA]_{max}\left(1 - \frac{d_i}{r}\right)\right\}, \quad [7]$$

where $[IAA]_{max}$ is the model maximum IAA concentration.

A possible molecular mechanism for the resulting bias of PIN1 protein polarization toward the primordium center might be a diffusing substance released by cells located at the center. This substance would be prevented from spreading outside the primordium by boundary cells. Another possibility might be a mechanical induction of PIN1 polarization, caused by stresses or strains in the primordium.

(*iii*) The concentration of auxin in a primordium is capped at a maximum level $[IAA]_{max}$, with the excess amount of auxin assumed to flow into the inner tissues of the primordium and initiate the vasculature.

Smith *et al.*

Fig. 4. Simulated shoot apical meristems. (*A–D*) The arrangement of primordia into phyllotactic patterns: distichous (*A*), decussate (*B*), tricussate (*C*), and spiral (*D*). (*E–G*) Simulated *pin1* mutant (*E*), primordium formed in the *pin1* mutant after localized application of auxin in the peripheral zone (*F*), and primordium ring formed in the *pin1* mutant after localized application of auxin at the tip of the apex (*G*). Arrows indicate the site of auxin application. (*H* and *I*) Simulated results of cell ablation: control apex (*H*) and the apex in which five cells shown in black have been removed (*I*). Note the shift in the position of the primordium initial (cells with high auxin concentration, shown in bright green) near the ablation site.

Simulation Results. We found that the postulated model of molecular control mechanisms, operating on a growing shoot apical meristem, can generate fundamental phyllotactic patterns: distichous, decussate, tricussate, and spiral (Fig. 4 *A–D*; see also Movies 1–4, which are published as supporting information on the PNAS web site). Parameter values used in the simulations are included in Table 1, which is published as supporting information on the PNAS web site. Sensitivity analysis indicates that the most critical component of the model is the exponential form of Eq. **2** for PIN1 polarization. In the case of spiral phyllotaxis, the choice of the exponentiation base *b* in Eq. **2** is also important (see sensitivity analysis in *Supporting Text*).

In our simulations, changes to multiple parameters were needed to obtain different phyllotaxis types. The simplest change, from distichous to decussate, involved increasing IAA production, de-

Fig. 5. Comparison of the divergence angles: angles measured in *Arabidopsis* with standard error bars (blue), and angles generated by the spiral phyllotaxis model (red).

creasing the width of the peripheral zone, and increasing the size of the central zone. The requirement for such complex changes may explain the almost universal failure to generate mutants that change one stable phyllotactic pattern into another (numerous unpublished results; for discussion see ref. 25).

In dicotyledonous plants, such as *Arabidopsis*, the embryo produces two cotyledons that arise near-simultaneously at angles close to 180°. From this decussate starting situation, a spiral phyllotaxis with divergence angles of ≈137.5° gradually emerges (26, 27). Our model recreates this pattern *de novo* within the standard error (Fig. 5). The spiral phyllotactic pattern is perpetuated if the simulation continues (Table 2, which is published as supporting information on the PNAS web site).

Further support for the model is offered by recreating mutant phenotypes and manipulated plants. Specifically, the *pin1* phenotype is characterized by the absence of primordia (28) and low *DR5::GFP* expression (Fig. 2*C*). Removing production of PIN1 in the model reproduces the inhibition of organ formation (Fig. 4*E*). However, the concentration of auxin appears to be higher than in the *pin1* mutant and more similar to NPA-treated apices (Fig. 2 *C* and *D*).

Local application of auxin in the peripheral zone of a *pin1* mutant produces an isolated primordium (figure 3*A* in ref. 10), whereas local application of auxin at the tip of the apex results in the formation of a ring-shaped primordium (figure 3*C* in ref. 10). These experimental results are reproduced by the model (Fig. 4 *F* and *G*). In contrast, our model does not capture the dependence of the primordium size on the amount of auxin; furthermore, the simulated ring consists of many separate primordia, as observed in the *pinoid* mutant (figure 3*F* in ref. 10). We attribute these shortcomings to the simplistic nature of the geometric algorithm defining position and scope of primordia in our model, rather than failure of the postulated molecular patterning mechanism.

Laser ablation of incipient primordium cells causes the emergence of a displaced primordium in the vicinity of the ablated site (figure 3 in ref. 29). This effect is reproduced in our model (Fig. 4 *H* and *I*).

Conclusions

We constructed a simulation model of shoot apical meristems that reproduces the phyllotaxis of *Arabidopsis* vegetative shoots. Our simulation model supports the basic tenet of the conceptual model proposed by Reinhardt *et al.* (10), according to which phyllotaxis results from the dynamics of interaction between existing and incipient primordia in a growing apex, mediated by actively trans-

ported auxin. New primordia emerge in the areas of high auxin concentration and maintain a distance from each other by depleting auxin in their proximity.

An important aspect of our model is the transport-based patterning mechanism, which involves a putative positive feedback loop between the concentration of auxin, the localization of PIN1, and the polar transport of auxin. We showed that this mechanism, combined with diffusion, can "break symmetry" of an approximately uniform auxin distribution and form a spatial pattern of auxin concentrations that is stable over time (Fig. 3). The magnitude and spacing of concentration maxima depend on model parameters. This patterning mechanism is fundamentally different from reaction-diffusion in that it postulates a controlled redistribution of an existing morphogen (auxin) in space, whereas reaction-diffusion postulates a controlled local production of two or more morphogens. The transport-based patterning is also different from canalization, which postulates a sustained polar transport of auxin along the gradient of its concentration (14, 30–33). In contrast, in our model, auxin is preferably pumped toward the neighboring cell with the highest auxin concentration.

Experimental data show that PIN1 proteins in the L1 layer of a wild-type *Arabidopsis* meristem are generally oriented toward the primordium initial, and the position of primordia coincides with the maxima of auxin concentration. The transport-based patterning mechanism is consistent with these data but, according to our simulations, does not generate phyllotactic patterns by itself. Therefore, we postulate an additional factor: differentiation of cells within primordia. The primordia cells are characterized by increased auxin concentration, enhanced polarization of PIN1 proteins in the L1 toward primordium centers, and export of auxin from the L1 toward the internal layers. All of these characteristics have a strong experimental basis (Fig. 2; ref. 10).

Our model suggests that phyllotaxis is not governed by a single mechanism, but represents a combined effect of several factors. This complexity may be needed in nature to generate phyllotactic patterns in the presence of noise. The small number of cells around the peripheral zone of the Arabidopsis apex limits the precision in primordia placement to ≈15° (360° divided by ≈24 cells). A robust mechanism is thus needed to initiate and maintain phyllotactic patterns despite a relatively large departure in the placement of individual primordia from their mathematically ideal positions. The problem of generation of phyllotactic patterns in the context of an irregular geometry was not considered in previous models, which assumed continuous or uniformly discretized space.

Assumptions of our model include the localization of auxin sources and the molecular mechanism of PIN1 protein localization in a cell. According to the model of Reinhardt *et al.* (10), auxin is produced outside the shoot apical meristem and is acropetally transported into the meristem through the L1. We were not able to recreate spiral phyllotactic patterns under these conditions and assumed a uniform production throughout the L1 in the peripheral zone instead, with an additional boost in the primordia. Also, our model postulates localization of PIN1 toward the neighboring cells with the highest auxin concentration but leaves open the question of what molecular mechanism may produce this localization.

The answers to these questions may lead to the integration of the model of phyllotaxis with a model of vasculature formation in the leaf and stem. Although both processes are mediated by auxin, the proposed mechanism of PIN1 polarization involved in phyllotaxis is almost opposite to the canalization mechanism proposed for veins (14, 30, 32, 33). It is thus interesting how these different mechanisms may be reconciled in the growing plant.

Materials and Methods

All *Arabidopsis thaliana* lines were in the Columbia background. The *pin1* mutant allele used was *pin1-7*. *DR5::GFP* refers to the *DR5rev::GFP* line described in ref. 12. Treatments with NPA and sirtinol, visualization by confocal microscopy, and determination of divergence angles are described in *Supporting Text*. Simulation models were implemented by using the vv programming environment (34). Further technical details are given in *Supporting Text*.

1. Steeves, T. A. & Sussex, I. M. (1989) *Patterns in Plant Development* (Cambridge Univ. Press, Cambridge, U.K.).
2. Hofmeister, W. (1868) in *Handbuch der Physiologischen Botanik*, eds. Bary, A. d., Irmisch, T. H. & Sachs, J. (Engelmann, Leipzig, Germany), pp. 405–664.
3. Snow, M. & Snow, R. (1932) *Philos. Trans. R. Soc. London B* **221**, 1–43.
4. Richards, F. J. (1951) *Philos. Trans. R. Soc. London B* **235**, 509–564.
5. Green, P. B., Steele, C. S. & Rennich, S. C. (1996) *Ann. Bot. (London)* **77**, 515–527.
6. Douady, S. & Couder, Y. (1996) *J. Theor. Biol.* **178**, 255–312.
7. Veen, A. H. & Lindenmayer, A. (1977) *Plant Physiol.* **60**, 127–139.
8. Meinhardt, H., Koch, A.-J. & Bernasconi, G. (1998) in *Symmetry in Plants*, eds. Barabe, D. & Jean, R. V. (World Scientific, Singapore), pp. 723–758.
9. Reinhardt, D., Mandel, T. & Kuhlemeier, C. (2000) *Plant Cell* **12**, 507–518.
10. Reinhardt, D., Pesce, E. R., Stieger, P., Mandel, T., Baltensperger, K., Bennett, M., Traas, J., Friml, J. & Kuhlemeier, C. (2003) *Nature* **426**, 255–260.
11. Stieger, P. A., Reinhardt, D. & Kuhlemeier, C. (2002) *Plant J.* **32**, 509–517.
12. Benková, E., Michniewicz, M., Sauer, M., Teichmann, T., Seifertova, D., Jurgens, G. & Friml, J. (2003) *Cell* **115**, 591–602.
13. Casimiro, I., Marchant, A., Bhalerao, R. P., Beeckman, T., Dhooge, S., Swarup, R., Graham, N., Inze, D., Sandberg, G., Casero, P. J. & Bennett, M. (2001) *Plant Cell* **13**, 843–852.
14. Rolland-Lagan, A.-G. & Prusinkiewicz, P. (2005) *Plant J.* **44**, 854–865.
15. Dai, X., Hayashi, K., Nozaki, H., Cheng, Y. & Zhao, Y. (2005) *Proc. Natl. Acad. Sci. USA* **102**, 3129–3134.
16. Woodward, A. W. & Bartel, B. (2005) *Ann. Bot. (London)* **95**, 707–735.
17. Ljung, K., Bhalerao, R. P. & Sandberg, G. (2001) *Plant J.* **28**, 465–474.
18. Weijers, D., Sauer, M., Meurette, O., Friml, J., Ljung, K., Sandberg, G., Hooykaas, P. & Offringa, R. (2005) *Plant Cell* **17**, 2517–2526.
19. Vieten, A., Vanneste, S., Wisniewska, J., Benková, E., Benjamins, R., Beeckman, T., Luschnig, C. & Friml, J. (2005) *Development (Cambridge, U.K.)* **132**, 4521–4531.
20. Paciorek, T., Zazimalova, E., Ruthardt, N., Petrasek, J., Stierhof, Y. D., Kleine-Vehn, J., Morris, D. A., Emans, N., Jurgens, G., Geldner, N. & Friml, J. (2005) *Nature* **435**, 1251–1256.
21. Mattsson, J., Ckurshumova, W. & Berleth, T. (2003) *Plant Physiol.* **131**, 1327–1339.
22. Kang, J. & Dengler, N. (2002) *Planta* **216**, 212–219.
23. Elliott, R. C., Betzner, A. S., Huttner, E., Oakes, M. P., Tucker, W. Q., Gerentes, D., Perez, P. & Smyth, D. R. (1996) *Plant Cell* **8**, 155–168.
24. Turing, A. (1952) *Philos. Trans. R. Soc. London B* **237**, 5–72.
25. Kuhlemeier, C. & Reinhardt, D. (2001) *Trends Plant Sci.* **6**, 187–189.
26. Mündermann, L., Erasmus, Y., Lane, B., Coen, E. & Prusinkiewicz, P. (2005) *Plant Physiol.* **139**, 960–968.
27. Callos, J. D. & Medford, J. I. (1994) *Plant J.* **6**, 1–7.
28. Okada, K., Ueda, J., Komaki, M. K., Bell, C. J. & Shimura, Y. (1991) *Plant Cell* **3**, 677–684.
29. Reinhardt, D., Frenz, M., Mandel, T. & Kuhlemeier, C. (2005) *Development (Cambridge, U.K.)* **132**, 15–26.
30. Mitchison, G. J. (1981) *Philos. Trans. R. Soc. London B* **295**, 461–471.
31. Feugier, F. G., Mochizuki, A. & Iwasa, Y. (2005) *J. Theor. Biol.* **236**, 366–375.
32. Mitchison, G. J. (1980) *Philos. Trans. R. Soc. London B* **207**, 79–109.
33. Sachs, T. (1981) *Adv. Bot. Res.* **9**, 151–262.
34. Smith, C., Prusinkiewicz, P. & Samavati, F. (2003) *Lecture Notes in Computer Science* (Springer, Berlin) Vol. 3062, pp. 313–327.